Atomic arrangement and emission properties of GaAs(In, Sb)N quantum wells

2009 Semicond. Sci. Technol. 24 075013

(http://iopscience.iop.org/0268-1242/24/7/075013)

Semicond. Sci. Technol. **24** (2009) 075013 (8pp) doi:10.1088/0268-1242/24/7/075013

Atomic arrangement and emission properties of GaAs(In, Sb)N quantum wells

A M Mintairov[1], K Sun[1], J L Merz[1], H Yuen[2], S Bank[2], M Wistey[2], J S Harris[2], G Peake[3], A Egorov[4], V Ustinov[4], R Kudrawiec[5] and J Misiewicz[5]

[1] University of Notre Dame, Notre Dame, IN 46556, USA
[2] Stanford University, Stanford, CA 94305, USA
[3] Sandia National Laboratories, Albuquerque, NM 87185, USA
[4] Ioffe Physico-Technical Institute, St Petersburg, Russia
[5] Institute of Physics, Wroclaw University of Technology, Wroclaw, Poland

Received 1 December 2008, in final form 1 May 2009
Published 5 June 2009
Online at stacks.iop.org/SST/24/075013

Abstract
Fine structure related to different types of atomic arrangements (short-range order, phase separation and quantum dots) was observed in high-spatial-resolution low-temperature photoluminescence (PL) spectra of GaAsInN, GaAsSbN and GaAsInSbN quantum wells (QWs) containing ∼1.5% N and emitting at 1.2–1.3 μm. Using photoreflectance and temperature-dependent PL spectroscopy, we measured the activation energies and band-tail width of localized states, associated with different atomic arrangements, to be 5–66 meV. We found that the emission intensity in these GaAs(In, Sb)N QWs weakly depends on carrier localization and that it is limited at cryogenic temperatures by exciton scattering by *N* interstitials, while at room temperature it is limited by an intrinsic non-radiative recombination channel having activation energy of ∼60 meV and capture time between 0.01 and 1 ps.

(Some figures in this article are in colour only in the electronic version)

1. Introduction

The incorporation of small amounts of nitrogen (up to 5%) into III–V materials (GaAs, InGaAs and GaAsSb) leads to anomalously strong reduction of the band gap [1–3], which is very attractive for GaAs-based optoelectronics devices operating in the near-infrared spectral range [4, 5]. Arising from specific chemical properties of nitrogen, such as its large electronegativity and small size [6, 7], the strong reduction of the band gap in such dilute nitride alloys creates an extremely large energy scale for statistical compositional fluctuations or, in other words, wide disorder-induced band tails. The resulting strong electron localization leads to a variety of effects, including enhanced spectral broadening of optical transitions and Stokes shift [8], the appearance of a so-called S-shape temperature dependence of the photoluminescence (PL) peak position at low temperature [9], reduced minority carrier diffusion lengths [10] and reduced electron mobility [11]. At the same time the chemical properties and bonding of nitrogen lead to intrinsic non-radiative defects, which are absent in conventional III–V materials [12–18]. The non-radiative centers, which include *N* interstitials [15–17], As antisites [14] and Ga vacancies [18], are responsible for strong temperature quenching of the PL of as-grown material and require post-growth annealing [13–18]. Both carrier localization and non-radiative defects dramatically affect transport and optical properties of dilute nitrides and need to be controlled for device applications.

Two kinds of dilute nitride structures with nitrogen composition 1–3% are used as active layers for near-infrared applications: one, having band gaps ∼1.2 eV (emission wavelength $\lambda \sim 1$ μm), is tensively strained GaAsN and lattice-matched GaAsInN and GaAsSbN epi-layers having In and Sb compositions below 10% and the other, having band gaps down to 0.8 eV ($\lambda \sim 1.5$ μm), is compressively strained GaAsInN and GaAsSbN quantum wells (QWs) with In and Sb compositions up to 40%. Recently, GaAsInSbN QWs were

also used for long wavelength ($\lambda = 1.3$–1.5 μm) applications, in which the incorporation of small amounts of Sb (up to 2%) into GaAsInN QWs was used to improve structural uniformity [19].

It has been shown using high spatial resolution near-field photoluminescence that in GaAsN and GaAsInN epi-layers with band gaps ∼1.2 eV, the strong carrier localization is accompanied by formation of quantum-dot-like composition fluctuations [20]. Such intrinsic quantum dots (QDs) have size ∼15 nm, activation energy ∼30 meV and density ∼100 μm^{-3}, which imply their spontaneous formation, i.e. phase separation (PS) effects. The existence of QDs suppressing the lateral carrier transport to non-radiative traps can improve luminescent characteristics of dilute nitrides but at present little is known about the formation of intrinsic QDs and their effect on the emission mechanism in long wavelength GaAsInN, GaAsSbN and GaAsInSbN used for light emitting devices. On the other hand, it was found that electronic states of GaAsInN QWs at In composition >20% were greatly affected by short-range order (SRO) nitrogen arrangements, creating discrete band gaps for $Ga_nIn_{4-n}N$ ($n = 0$–4) nearest-neighbor environments with energy splitting ∼20 meV [21].

In this paper, we used high spatial resolution photoluminescence (HSR-PL) spectroscopy to probe QD formation, SRO and PS atomic arrangements and structural uniformity of GaAsInN, GaAsSbN and GaAsInSbN QWs emitting at 1.2–1.3 μm and we apply conventional PL and photoreflectance spectroscopy to study the effect of structural uniformity and carrier localization on radiative process in these GaAs(In, Sb)N QWs. We found a strong suppression of QD formation and dominance of SRO or long-range PS in these QWs. We measured the activation energies and band-tail width of localized states, associated with different atomic arrangements, to be 5–66 meV. We found that the emission intensity in these GaAs(In, Sb)N QWs weakly depends on carrier localization. We show that their emission intensity is limited at cryogenic temperatures by exciton scattering by N interstitials, while at room temperature it is limited by an intrinsic non-radiative recombination channel having activation energy of ∼60 meV and capture time between 0.01 and 1 ps.

2. Experimental details

In this work we report results on as-grown and annealed GaAsInN, GaAsSbN and GaAsInSbN QW samples having nitrogen composition ∼1.5% and the emission wavelengths at 300 K ($\lambda_{300\,K}$) ∼ 1.2–1.3 μm. While in our preliminary study we have measured several samples of each type, four representative samples, showing characteristic behavior, were chosen for the present study. The samples are GaAsInN1, GaAsInN2, GaAsSbN1 and GaAsInSbN2 QWs, where in sample notation the last number denotes as-grown (1) or annealed (2) sample. The In and Sb compositions for these samples, well thicknesses and references to details of their growth and annealing are presented in table 1. In the quaternary GaAsInN and GaAsSbN QWs, composition of In or Sb was of order 40%. In the quinary GaAsInSbN QW sample, the compositions of In and Sb were 30% and 2%, respectively. The well thickness is 6 or 7 nm. The GaAsSbN sample was grown by metal organic chemical vapor deposition (MOCVD) [22], while the rest of the samples were grown by molecular beam epitaxy (MBE). The energy gap between ground and first excited states in these QWs was found from photoreflectance measurements (see below) to be ∼100 meV. The annealing results in strong increase of emission intensity and energy shift. The shift has value 40–60 meV and is blue (red) for In (Sb) containing material.

Table 1. GaAs(In, Sb)N QW samples ($N \sim 1.5\%$)[a].

Samples	In(Sb) composition, %	d, nm	Growth details	Annealing
GaAsInN1	40(0)	6	[20]	No
GaAsInN2	40(0)	6	[20]	Yes
GaAsInSbN2	30(2)	7	[19]	Yes
GaAsSbN1	0(50)	6	[22]	No

[a] Two reference QD samples were studied: (1) GaAsN QW ($N \sim 1.5\%$, $\lambda_{300\,K} \sim 1.0$ μm) with thickness 10 nm and (2) InAs/AlGaAs QD having $\lambda_{300\,K} \sim 1.2$ μm.

Four GaAs(In, Sb)N QW samples were compared with two reference samples for which the formation of intrinsic QDs was well established. These reference samples are (1) a GaAsN QW sample ($N \sim 1.5\%$, $\lambda_{300\,K} \sim 1.0$ μm) with thickness of 10 nm, having a dot size (density) of 12 nm (30 dots μm^{-2}) and activation energy of 30 meV [20] and (2) an InAs QD sample having $\lambda_{300\,K} \sim 1.2$ μm, dot size (density) of 12 nm (200 dots μm^{-2}) and activation energy of 450 meV [23]. The InAs QD sample represents an extreme case of carrier localization in which lateral transport of photoexcited carriers is suppressed and in which only well-defined localized centers (QDs) contribute to emission up to room temperature.

HSR-PL spectra were taken using μ-PL through metallic apertures having diameters 200–700 nm deposited directly on the samples using e-beam lithography. The μ-PL setup consists of an imaging module attached to a 270 mm focal length spectrometer and nitrogen-cooled InGaAs multichannel detector. The self-made imaging module, which enables simultaneous observation of the sample surface and laser spot focused to a diameter of a few μm, includes a micro-objective, beam-splitter and Olympus microscope illuminator with a CCD camera. We also used a conventional PL setup with the exciting laser focused on a spot of ∼100 μm. We used an excitation wavelength of 488 nm from an Ar ion laser, with excitation power densities $P = 0.1$–1000 W cm^{-2}. Temperature-dependent measurements were performed in the range 10–300 K using a liquid helium flow cryostat. We used Gaussian contour modeling provided by graphic plot Origin software to separate different spectral components and to measure integral intensity of PL bands.

The details of the photoreflectance (PR) technique and the analysis of the PR spectra are previously described [24].

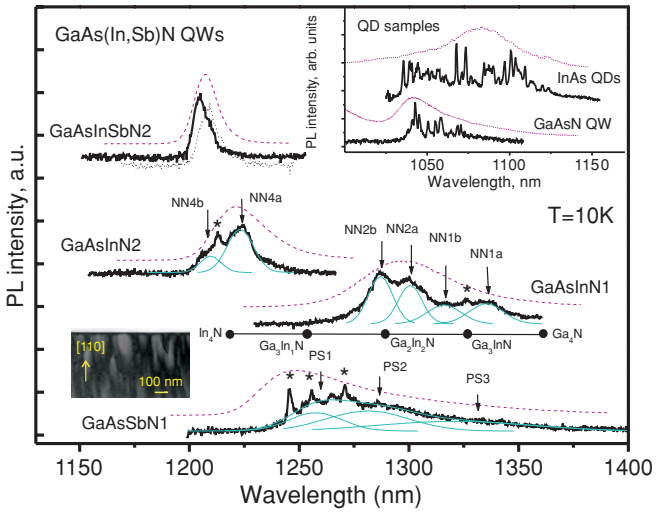

Figure 1. Comparison of HSR spectra (thick solid curves and dotted curve for GaAsInSbN2 QW) and macro-PL spectra (dashed curves) of four GaAs(In, Sb)N samples. The thin solid curves are individual components of multiple Gaussian peak decomposition of the HSR spectra line shape, excluding sharp features denoted by stars (for GaAsSbN1 sample, the resulting contour is also shown). The upper right inset shows a comparison of HSR and macro-PL spectra for reference samples of GaAsN QW and InAs QDs. The spectra were measured at $T = 10$ K and power density 50 W cm^{-2}. Solid circles connected by the horizontal line show positions of band gaps of $Ga_nIn_{4-n}N$ ($n = 0$–4) nearest-neighbor SRO arrangements taken from [21]. The lower left image is a plain-view transmission electron microscopy image of GaAsSbN QW.

3. High spatial resolution photoluminescence spectra

Low-temperature HSR (spatial resolution 200 and 400 nm) spectra of the four GaAs(In, Sb)N QW samples are presented in figure 1. In the upper right inset of figure 1, HSR spectra of the two reference QD samples are shown. We also plot conventional macro-PL (spatial resolution ∼100 μm) spectra above each HSR one. The lower left inset is a plain-view transmission electron microscopy (TEM) image of GaAsSbN QW, revealing phase separation effects in this material. The power density for spectra in figure 1 is ∼50 W cm^{-2}. For each sample, we have measured few (up to five) different apertures of the same size. For annealed samples (GaAsInN2 and GaAsInSbN2) having high PL intensity at low temperature we were able to use 200 nm apertures, but for as-grown ones (GaAsInN1 and GaAsSbN1) reasonable signals were obtained only for 400 nm apertures. We observed shifts of spectral features of only few nanometers for different apertures, which we attribute to the long-scale fluctuation of the alloy composition. Such fluctuations usually smear out the fine structure of PL spectra at apertures >400 nm. In figure 1, we show the spectra using only one aperture for quaternary QWs GaAsInN1, GaAsInN2 and GaAsSbN1. For quinary GaAsInSbN2 QW, we present spectra using two different apertures.

In the structurally uniform quinary GaAsInSbN2 QW, a single PL peak having full width at half-maximum (FWHM) ∼8 meV is seen for both apertures. No sharp lines were observed in this sample. A 5 nm difference in peak position for these apertures is clearly seen. In the quaternary QWs GaAsInN1, GaAsInN2 and GaAsSbN1, the PL spectra become broader and the fine structure of the PL bands is resolved. To visualize individual components of this structure and estimate their width, we presented in figure 1 their Gaussian contours. The fine structure consists of several overlapping bands with FWHM 10–30 meV, on which a few sharp lines (FWHM ∼3 meV, indicated by stars in the figure) are superimposed. The observed sharp lines can be related to single N-rich QDs, which are also seen in the reference GaAsN QW sample (see the inset in figure 1). The number of lines observed is three for GaAsSbN (at 1246, 1256 and 1272 nm) and one for annealed (at 1212 nm) and as-grown (at 1325 nm) GaAsInN. These are far fewer than those observed in the reference GaAsN sample, which shows ∼10 lines, indicating suppression of QD formation in the quaternaries.

For In-free GaAsSbN1 QW, three bands with width 20–30 meV can be separated in HSR PL spectra. For particular aperture presented, the bands are centered at 1260, 1280 and 1330 nm and we denote them as PS1, PS1 and PS3 respectively. We assign these bands to emission of regions with different Sb compositions, i.e. to PS, as was established by our TEM measurements (see the left lower inset in figure 1), in which one-dimensional PS with spatial modulation ∼100 nm along one of {1 1 0} directions was observed.

For the In-containing quaternary samples GaAsInN1 and GaAsInN2, the broad overlapping bands reveal a clear doublet structure with energy splitting ∼10 meV. While a single doublet, denoted NN4a/NN4b, is observed in the GaAsInN2 sample, two doublets centered at 1290 and 1330 nm, denoted NN2a/NN2b and NN1a/NN1b, respectively, are seen in the GaAsInN1 sample. The doublet structure of HSR spectra of GaAsInN2 QWs can be clearly seen in comparison to the GaAsInSbN2 sample having nearly the same spectral position, in which only a single peak is observed. The observation of the single peak in the structurally uniform quinary material gives strong evidence that the doublet structure in the quaternary GaAsInN QWs reflects the fluctuations of well thickness on the length scale 200–400 nm (aperture size). The doublets NN1a/NN1b, NN2a/NN2b and NN4a/NN4b can be related to the following SRO atomic arrangements, i.e. configurations of cations surrounding an isolated nitrogen atom: Ga_3In_1N, Ga_2In_2N and In_4N, respectively. This follows from the fact that the energy positions and energy separation between these bands remarkably well agree with the energy positions and energy separations between corresponding SRO bands (also presented in figure 1)[6] previously observed in photoreflectance spectra in similar GaAsInN QWs in [21]. Thus in as-grown GaAsInN1 QW, Ga_3In_1N and Ga_2In_2N SRO atomic arrangements are dominated. Annealing is accompanied by diffusion of nitrogen atoms from Ga to In (see also [25] on the effect of QW interdiffusion) and formation of In_4N SRO, which results in a 60 meV blue shift of PL spectra in GaAsInN2

[6] In plotting of $Ga_nIn_{4-n}N$ microcluster conduction band energies, we used supercell calculation results presented in [21] to actual In composition of 40% of our samples.

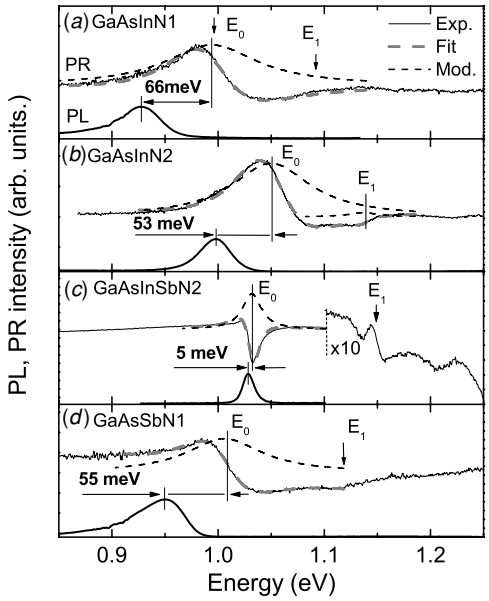

Figure 2. Experimental PR and PL spectra (solid curves) of GaAs(In, Sb)N QWs together with PR spectra simulations (thick dashed curves). Thin dashed curves represent the module of the PR resonance transition contribution.

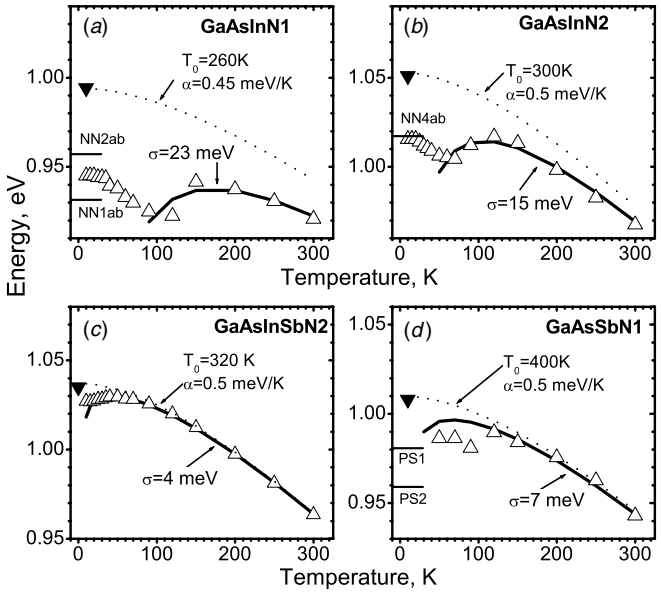

Figure 3. Temperature dependence of PL peak position (open triangles), band-tail model [28] (thick solid curves) and the Varshni band-gap model (thin dotted curves) for GaAs(In, Sb)N QWs. The solid inverted triangle at 10 K is the energy E_0 in each case. The horizontal lines are the energies of the fine structure components of the HSR spectra. The power density is 50 W cm^{-2}.

QW. Our results using HSR spectra allow us connect a carrier localization in the GaAs(In, Sb)N QWs to specific SRO and PS atomic arrangement, i.e. reveal microscopic origin of carrier localization.

4. Carrier localization in macro-photoluminescence and photoreflectance spectra

Macroscopically carrier localization is characterized by a Stokes shift, i.e. by offset of absorption and emission peaks, and by a band-tail dispersion. For a random alloy, the band-tail density of states is described by the Gaussian function. A topographical theory of random interface disorder in QWs [26] leads to a universal ratio of the Stokes shift to the exciton absorption linewidth $a = 0.553$. This ratio follows from statistical properties of the Gaussian random distribution function and reflects the fact that the emission spectrum of the band tail is related to the distributions of heights of local minima, while the optical absorption spectrum is related to the density of local minima itself. In conventional III–V and II–VI semiconductor alloys, the a values were found to be very close to the theoretical value for two orders of magnitude of PL linewidth values [26] and we did not find in the literature the estimation of this value for dilute nitrides.

In figures 2(*a*)–(*d*) we present low temperature PL and PR spectra, and in figures 3(*a*)–(*d*) we present temperature shift of the PL peak, which we used to measure the carrier localization parameters in our GaAs(In, Sb)N QW.

In figures 2(*a*) and (*b*) the PR spectra show the intensity oscillations related to ground (E_0) and excited (E_1) state QW transitions in the range 0.99–1.15 eV, and the PL spectra show a single peak shifted to lower energies of the E_0 PR resonance. The energy (E_0) and width (γ_{PRLT}) of the ground-state transition was obtained from standard fitting of the PR resonances using the formula from [27]:

$$\frac{\Delta R}{R}(E) = \mathrm{Re}[C \cdot \mathrm{e}^{\mathrm{i}\cdot\vartheta}(E - E_0 + i \cdot \Gamma)^{-m}], \qquad (1)$$

where C and ϑ are the amplitude and phase of the line, respectively, and $m = 2$. The fitting curves are shown by thick gray dashed lines in figures 2(*a*)–(*d*) together with the moduli of individual resonances (dashed lines). Accounting for the fact that the main contribution to the photo-modulated signal results from mobile carriers, we assign the energy transitions E_0 determined from the PR spectra to a mobility edge. The energy difference between E_0 and PL peak maxima corresponds to the Stokes shift or activation energy (E_{ac}). We should point out that since the PL spectra probe the band-tail states filled by photo-excitation, they depend on excitation power. Such band-filling (BF) effects lead to excitation power dependence of E_{ac}. For a power density range from 0.1 to 1000 W cm^{-2}, the energy shift of the PL peak ($-\Delta E_{\mathrm{ac}}$) at 10 K has values 40 meV for GaAsSbN1, 25 meV for both GaAsInN samples and 3 meV for GaAsInSbN2.

In figures 3(*a*)–(*d*), we plot the PL peak shift versus temperature (in the range 10–300 K) together with the mobility edge (E_0) and the positions of the fine structure peaks from the HSR PL at 10 K. The latter allow us to see the activation energy for discrete microscopic localized states, related to SRO and PS atomic arrangements. In figures 3(*a*)–(*d*), we also present the results of the analysis of the PL peak temperature shift using the band-tail model of Eliseev [28]. According to this model, the shift of PL peak maxima is described by the expression

$$E_{\mathrm{PL}}(T) = E_g(T) - \sigma^2/kT, \qquad (2)$$

where $E_g(T) = E_0 - \frac{\alpha T^2}{T_0+T}$ is the normal temperature dependence of the band gap (Varshni model), σ is a Gaussian

Table 2. Carrier localization parameters of GaAs(In, Sb)N QW obtained from optical spectra.

Sample	Activation energy (E_{ac})[a], meV	PR peak width (γ_{PRLT}), meV	PL peak width[b] (γ_{PLLT}), meV	Band-tail width (γ_{BTM}), meV
GaAsInN1	66	106	35	54
GaAsInN2	53	90	20	35
GaAsInSbN2	5	20	11	9
GaAsSbN1	55	87	41	16

[a] For power density 0.1 W cm^{-2}.
[b] For GaAsN QW and InAs QD sample $\gamma_{PLLT} = 25$ and 45 meV.

dispersion of a band-tail density of states and k is the Boltzmann constant. The above expression is valid for nondegenerate carrier occupation, which does not hold at very low temperatures. According to the band-tail model the PL peak has a 'blue' shift up to temperature T_1, below which $\sigma^2/kT > E_g(T) - E_0$, and then for $T > T_1$ it has a red shift. Such a behavior can be observed in the experimental data in figures 3(*a*)–(*d*) with T_1, ranging from 50 K for GaAsInSbN2 to 150 K for GaAsInN1. Note that the experimental data follow the thick solid curves (band-tail model), increasing with increasing temperature to T_1 and then decreasing at higher temperature. The data in figures 3(*a*)–(*d*) also reveal the so-called S-shape dependence, which manifests itself by an initial red shift from $T = 10$ K to temperature T_2 ($T_2 < T_1$), which corresponds to a non-equilibrium carrier population [29, 30]. In figures 3(*a*)–(*d*), one can see that T_2 varies from 20 K for GaAsInSbN2 to 100 K for as-grown GaAsInN1. For known $E_g(T)$ (see [31] for the GaAsInN QW sample), the dispersion σ (or the band-tail band width $\gamma_{BTM} = 2.35\sigma$) is the only fitting parameter of the model. The fitting curves $E_{PL}(T)$ and the band gap $E_g(T)$ are shown by solid and dashed curves, respectively, together with fitting parameter σ and band-gap parameters α and T_0 in figures 3(*a*)–(*d*). The parameters α and T_0, having values 0.5 meV K^{-1} and 260–400 K, were taken from [31] and were then adjusted for each sample to obtain a better fit.

The quantities obtained from the data in figures 2(*a*)–(*d*) and 3(*a*)–(*d*), i.e. the activation energy (E_{ac}), the PR (γ_{PRLT}) and PL (γ_{PLLT}) FWHM and the band-tail-model width (γ_{BTM}), are presented in table 2. One can see from table 2 that high structural uniformity of GaAsInSbN2 QW corresponds to E_{ac} value as low as 5 meV, i.e. to weak localization. For the rest of QWs the activation energy is an order of magnitude larger (∼55 meV), so they have strong carrier localization, which results from structural disorder induced by SRO or PS and from interface fluctuations. The quantities related to the band-tail dispersion, i.e. γ_{PLLT}, γ_{PRLT} and γ_{BTM}, are proportional to activation energies in most cases. For all samples both the PL-peak and band-tail-model widths are much narrower (two–four times) than the width of the PR resonance ($\gamma_{PRLT}/\gamma_{PLLT} \sim \gamma_{PRLT}/\gamma_{BTM} \sim$ 2–4), which is related to BF.

We can connect the weak carrier localization in quinary GaAsInSbN2 QW to improved interface roughness induced by antimony incorporation, uniformity of short-range atomic arrangements and suppression of nitrogen-induced PS, i.e. QD formation. Very weak nitrogen PS in this sample follows from the fact that the observed value of γ_{PLLT} (11 meV) is close to an estimated value of the excitonic PL linewidth for random GaAsN with $N \sim 1.5\%$ ($\gamma_{randomN} \sim 8$ meV) [32]. Note that for pure GaAsN QW, having nitrogen PS, i.e. QDs, the PL linewidth is twice larger (see figure 1 and table 2). The width of the fine structure peaks in GaAsInN QWs $\gamma_{HSR\text{-}PL} \sim$ 10 meV indicates suppression of nitrogen-induced PS. In these QWs, the PL width and carrier localization are determined by SRO and interface fluctuations. In GaAsSbN QW, $\gamma_{HSR\text{-}PL} \sim$ 25 meV and nitrogen and antimony PS coexist and both determine carrier localization.

For GaAsInSbN2 QW, the ratio of Stokes shift to absorption width $a = E_{ac}/\gamma_{PRLT}$ has value 0.25, which is nearly twice smaller than predicted for random interface fluctuations and which, thus, can manifest dominance of compositional disorder in that material having weak localization. For quaternary GaAsInN and GaAsSbN QWs, having strong localization the ratio $E_{ac}/\gamma_{PRLT} \sim 0.6$ is close to theoretical prediction for interface fluctuations disorder and thus is not sensitive to microscopic origin of compositional disorder (SRO or PS). On the other hand, the band-tail width γ_{BTM} obtained from PL temperature shift seemed to be sensitive to atomic arrangement, and an anomalously small γ_{BTM} value for GaAsSbN1 QW (16 meV) can reflect antimony PS effect in this material.

Our samples representing different localization energies and atomic arrangements were used for measurements of integral PL intensity at different temperatures, which allow us to study effect of compositional fluctuations and non-radiative recombination centers on luminescent properties of GaAs(In, Sb)N QWs.

5. Emission mechanism

Figures 4(*a*) and (*b*) show the dependence of the integral PL band intensity of the four GaAs(In, Sb)N QW samples, and the InAs QD reference sample, in the temperature range 10–300 K for two excitation powers $P_1 = 50$ and $P_2 = 1000$ W cm^{-2}. The intensity is plotted on a logarithmic scale versus reciprocal temperature (Arrhenius plot) and fitted (for QWs) by an expression describing the thermal activation of i non-radiative channels having activation energies E_i and capture times τ_i [33–35]:

$$I_{PL}(T) = I_0 \left[1 + \sum_i \frac{\tau_0}{\tau_i} e^{-E_i/kT} \right]^{-1}, \qquad (3)$$

where τ_0 is the radiative lifetime. One can see from figures 4(*a*) and (*b*) that for In-containing GaAsInN1, GaAsInN2 and GaAsInSbN2 QWs, the PL intensity decreases

Table 3. Thermal activation parameters of non-radiative channels in GaAs(In, Sb)N QWs[a].

Sample	Atom arrangement	Channel S		Channel D	
		Energy (E_S), meV	Capture time (τ_S)[b], ps	Energy (E_D), meV	Capture time (τ_D)[b], ps
GaAsInN1	SRO Ga_4N/Ga_3In_1N	8	300	55	1–5
GaAsInN2	SRO Ga_1In_3N/In_4N	8	100–200	65	0.01–0.1
GaAsInSbN2	SRO Ga_1In_3N/In_4N	6	50–120	55	0.1–3
GaAsSbN1	PS Sb	5	70	60	3-∞

[a] The excitation density is $P_1 = 50$ and $P_2 = 1000$ W cm^{-2}, giving a range of capture times from short (at P_1) to longer (at P_2).
[b] Calculated for radiative lifetime $\tau_0 = 1$ ns.

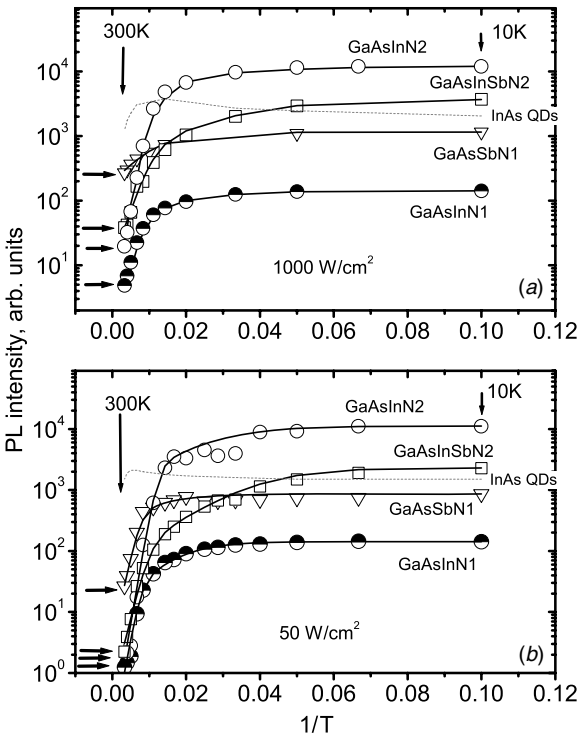

Figure 4. The integral intensity of the PL spectra versus temperature (circles, triangles and squares) and an Arrhenius plot fitting (solid curves) for GaAsInN1 (half-filled circles), GaAsSbN1 (inverted triangles), GaAsInSbN2 (squares) and GaAsInN2 (solid circles) QW samples, measured at power density: (*a*) 1000 W cm^{-2} and (*b*) 50 W cm^{-2}. Dashed curves are experimental data for the reference InAs QD sample.

in the temperature range 10–300 K by more than order of magnitude for both values of P. One can also see that this decrease (the intensity ratio $I^{10\,K}/I^{300\,K}$) decreases with the power density increase, which manifests BF effects. The strongest drop of the PL intensity is observed for GaAsInN2 QW having $I^{10\,K}/I^{300\,K} \sim 5000$ at P_1 and ~500 at P_2. On the other hand for In-free GaAsSbN1 QW, the intensity ratio $I^{10\,K}/I^{300\,K}$ is much smaller: ~30 at P_1 and ~3 at P_2. In contrast to dilute nitride QWs, the InAs QDs show negligible temperature intensity changes for both P_1 and P_2, thus indicating the absence of the contribution of non-radiative channels in the emission process.

Table 3 contains E_i and τ_i values obtained from the fitting. The scattering times τ_i were calculated using the averaged value of radiation lifetime $\tau_0 = 1$ ns, obtained from our unpublished time-resolved measurements (see also [36, 37]) for weakly localized states ($E_{ac} \sim 10$ meV). We should also point out that in the band tail ($E_{ac} > 10$ meV) τ_0 increases with increasing localization energy [34, 35], which is a result of the decreasing exciton localization volume [38] and which can be partly responsible for excitation power dependence of τ_i. For all GaAs(In, Sb)N QWs, two types of channels are obtained. The shallow, S-channel, having $E_S = 5$–8 meV and $\tau_S \sim 100$ ps, is responsible for PL intensity decrease in the range 10–50 K, while the deep, D-channel, having $E_D = 55$–65 meV and $\tau_D \sim 0.01$–1 ps, is responsible for PL intensity decrease at higher temperatures.

As can be seen from table 3, the GaAsInN2 and GaAsInSbN2 samples have the shortest capture times for the D-channel ($\tau_D \ll 1$ ps at P_1) and the GaAsSbN1 sample has the longest ($\tau_D = 3$ ps at P_1). This corresponds to nearly an order of magnitude stronger PL intensity of the GaAsSbN1 QW sample at 300 K. This gives strong evidence that the non-radiative defects identified in dilute nitrides, such as *N* interstitials [15–17], As antisites [14] and Ga vacancies [18], and which are suppressed (increase of τ_i) by annealing (note that GaAsInN2 and GaAsInSbN are annealed samples) do not contribute to the non-radiative channel D. On the other hand, at 10 K the annealed GaAsInN2 and GaAsInSbN2 QWs have much stronger intensity than as-grown GaAsInN1 and GaAsSbN1 QWs, which correlate with expected annealing of the above-mentioned defects.

We suggest that *N* interstitials, which have the highest density, and which are less sensitive to growth conditions, determine the PL intensity of GaAs(In, Sb)N QWs at low temperature. Since *N* interstitials are supposed to be deep ($E_A \sim 0.4$ eV [12]) they are not activated at the temperatures studied, but they can act as scattering centers, decreasing an exciton localization volume. The exciton localization volume of GaAs(In, Sb)N QWs and, thus, the density of the scattering centers can be determined by comparison of their PL intensity with the intensity of the InAs QD sample, for which exciton localization volume is known (~300 nm^3) [22]. Thus, an order of magnitude lower intensity of the GaAsInN1 sample compared to InAs QD in figures 4(*a*) and (*b*) gives exciton localization volume ~30 nm^3. This is in a good agreement with the density of *N* interstitials ~5×10^{19} cm^{-3} found in as-grown GaAsN [16, 17], which corresponds to localization

volume of 20 nm^3. Two orders of magnitude increase of PL intensity of GaAsInN2 compared to GaAsInN1 show expected annealing of these defects.

Our data show that in order to achieve strong emission efficiency of GaAs(In,Sb)N QWs at room temperature, important for device application, the D-channel must be suppressed. The nature of this channel is not known at the present time and we suppose that it corresponds to some phonon activated process, accounting for the fact that its activation energy is close to the energy of an optical phonon induced by nitrogen [39]. The D-channel can include scattering of the photogenerated carriers by optical phonons, reducing an effective emission volume. Similarly, the S-channel can be attributed to acoustic phonon activation processes, accounting for the fact that its activation energy is close to the acoustic phonon energies and that the capture times of S- and D-channels scale inversely with the activation energy. In our opinion, phonon-assisted non-radiative mechanisms manifest themselves as enhanced electron–phonon interactions in dilute nitride materials, arising from strong lattice distortion induced by the small size of the nitrogen. Some evidence confirming the importance of the contribution of the local lattice distortion and thus on the phonon-assisted mechanisms of the non-radiative channels S and D can be found in the fact that samples having preferential In–N bonds (GaAsInN2 and GaAsInSbN2) have shorter τ_D times than samples with preferential Ga–N bonding (GaAsInN1 and GaAsSbN1), and that Sb-free samples have longer τ_S times. The dependence of the non-radiative scattering times on bonding and atomic arrangements might provide a way to engineer better emission properties for GaAs(In, Sb)N QW samples.

6. Conclusion

We report the use of high spatial resolution photoluminescence (HSR-PL) spectroscopy to probe the formation of quantum dots (QDs), short-range atomic arrangements and structural uniformity of GaAsInN, GaAsSbN and GaAsInSbN QWs emitting at 1.2–1.3 μm. We found a strong suppression of QD formation in these QWs, unlike samples emitting at $\sim$1 μm reported earlier [20]. The quinary sample containing In and a few per cent of Sb appears to be by far the most uniform, in agreement with [19]. We also apply conventional PL spectroscopy and photoreflectance to study the effect of carrier localization (structural uniformity) and the non-radiative centers on luminescence properties of these GaAs(In, Sb)N QWs. We found that the emission intensity in these GaAs(In, Sb)N QWs weakly depends on carrier localization and that it is limited at cryogenic temperatures by exciton scattering by *N* interstitials, while at room temperature it is limited by an intrinsic non-radiative recombination channel having activation energy and capture time of $\sim$60 meV and 0.01–1 ps, respectively.

Acknowledgments

We wish to thank Dmitri Yakovlev for providing time-resolved measurements, Thomas Kosel for transmission electron microscopy measurements and Alexander Efros for helpful discussions. This work has been partially supported by a subaward under NSF/DMR06-06406.

References

[1] Weyers M, Sato M and Ando H 1992 *Japan. J. Appl. Phys.* **31** L853
[2] Kondo M, Uomi K, Niwa A, Kitatani T, Watahiki S and Yazawa Y 1996 *Japan. J. Appl. Phys.* **35** 1273
[3] Ungaro G, Le Roux G, Teisser R and Harmand J C 1999 *Appl. Phys. Lett.* **35** 1246
[4] Geiz J F, Friedman D J, Olson J M, Kurtz S R and Keyers B M 1998 *J. Cryst. Growth* **195** 401
[5] Livshits D A, Egorov A Y and Riechert H 2000 *Electron. Lett.* **36** 1025
[6] Sakai S, Ueda Y and Terauchi Y 1993 *Japan. J. Appl. Phys.* **32** 4413
[7] Wei S-H and Zunger A 1996 *Phys. Rev. Lett* **76** 664
Belaiche L and Zunger A 1998 *Phys. Rev. Lett.* **57** 4425
Kim K and Zunger A 2001 *Phys. Rev. Lett.* **86** 2609
[8] Buyanova I A, Chen W M, Pozina G, Monemar B, Xin H P and Tu C W 1999 *Phys. Status Solidi* b **216** 125
[9] Gernouillet L, Bru-Chevallier C, Guillot G, Gilet P, Duvaut P, Vannuffel C, Million A and Chenevas-Paule A 2000 *Appl. Phys. Lett.* **76** 2241
[10] Kurtz S R, Allerman A A, Seager C H, Sieg R M and Jones E D 2000 *Appl. Phys. Lett.* **77** 400
[11] Reason M, Jin Y, McKay H A, Mangan N, Mao D, Goldman R S, Bai X and Kurdak C 2007 *J. Appl. Phys.* **102** 103710
[12] Zhang S B, Janotti A, Wei S-H and Van de Walle C G 2004 *IEE Proc. Optoelectron* **151** 369
[13] Spruytte S G, Coldren C W, Harris J S, Wampler W, Krispin P, Ploog K and Larson M C 2001 *J. Appl. Phys.* **89** 4401
[14] Chen W M, Buyanova I A and Tu C W 2004 *IEE Proc. Optoelectron* **151** 379
[15] Ramsteiner M, Jiang D S, Harris J S and Ploog K H 2004 *Appl. Phys. Lett.* **84** 1859
[16] Reason M, McKay H A, Ye W, Hanson S, Goldman R S and Rotberg V 2004 *Appl. Phys. Lett.* **85** 1692
[17] Ahlgren T, Vainonen-Ahlgren E, Likonen J, Li W and Pessa M 2002 *Appl. Phys. Lett.* **80** 2314
[18] Toivonen J, Hakkarainen T, Sopanen M, Lipsanen H, Oila J and Saarinen K 2003 *Appl. Phys. Lett.* **82** 40
[19] Harris James S Jr *et al* 2007 *Phys. Status Solidi* b **244** 2707
[20] Mintairov A M, Kosel T H, Merz J L, Blagnov P A, Vlasov A S, Ustionov V M and Cook R E 2001 *Phys. Rev. Lett.* **87** 277401
Mintairov A M *et al* 2004 *Physica* E **21** 385
Merz J *et al* 2004 *IEE Proc. Optoelectron.* **151** 346
Mintairov A *et al* 2005 *Mater. Res. Soc. Symp. Proc.* (Warrendale, PA) vol **838E** p O3.1
[21] Klar P J, Gruning H, Koch J, Schafer S, Volz K, Stolz W, Heimbrodt W, Kamal Saadi A M, Lindsay A and O'Reilly E P 2001 *Phys. Rev.* B **64** 121203
[22] Peake G M, Waldrip K E, Hargett T W, Modine N A and Serkland D K 2004 *J. Cryst. Growth* **261** 398
[23] Tokranov V, Yakimov M, Katsnelson A, Lamberti M and Oktyabrsky S 2003 *Appl. Phys. Lett.* **83** 833
Oktyabrsky S, Lamberti M, Tokranov V, Agnello G and Yakimov M 2005 *J. Appl. Phys* **98** 053512
[24] Misiewicz J, Kudrawiec R, Ryczko K, Sęk G, Forchel A, Harmand J C and Hammar M 2004 *J. Phys.: Condens. Matter* **16** 3071
[25] Peng C S, Lui H F, Konttinen J and Pessa M 2005 *Appl. Phys. Lett.* **278** 259

[26] Yang F, Wilkinson M, Austin E J and O'Donnell K P 1993 *Phys. Rev. Lett.* **70** 323
[27] Aspnes D E 1973 *Surf. Sci.* **37** 418
[28] Eliseev P G 2003 *J. Appl. Phys.* **93** 5404
[29] Lourenco S A, Dias I F L, Duarte J L, Laureto E, Aquino V M and Harmand J C 2007 *Braz. J. Phys.* **37** 1212
[30] Sizov D S, Zavarin E E, Ledentsov N N, Lundin V V, Musikhin Yu G, Sizov V S, Suris R A and Tsatsul'nikov A F 2007 *Semiconductors* **41** 575
[31] Grenouillet L, Bru-Chevallier C, Guillot G, Gilet P, Duvaut P, Vannuffel C, Million A and Chenevas-Paule A 2000 *Appl. Phys. Lett.* **76** 2241
[32] Senger R T and Bajaj K K 2003 *J. Appl. Phys.* **94** 7505
[33] Bacher G, Schweizer H, Kovac J, Forchel A, Nickel H, Schlapp W and Losch R 1991 *Phys. Rev.* B **43** 9312
[34] Pinault M-A and Tournie E 2003 *Solid State Electron.* **47** 477
[35] Lourenco S A, Dias I F L, Pocas L C, Duarte J L, Oliveira J B B and Harmand J C 2003 *J. Appl. Phys.* **93** 4475
[36] Buyanova I A, Pozina G, Hai P N, Thinh N Q, Bergman J P, Chen W M, Xin H P and Tu C W 2000 *Appl. Phys. Lett.* **77** 2325
[37] Krestnikov I L, Heitz R, Ledentsov N N, Hoffmann A, Mintairov A M, Kosel T H, Merz J L, Sosnikov I P and Ustinov V M 2003 *Appl. Phys. Lett.* **83** 3728
[38] Efros Al L, Wetzel C and Worlock J M 1995 *Phys. Rev.* B **52** 8384
[39] Mintairov A M, Blagnov P A, Melehin V G, Faleev N N, Merz J L, Qui Y, Nikishin S A and Temkin H 1997 *Phys. Rev.* B **56** 15836–41